Hindawi
Journal of Nanomaterials
Volume 2019, Article ID 3959037, 13 pages
https://doi.org/10.1155/2019/3959037

Research Article

PEGylation of Ginsenoside Rg3-Entrapped Bovine Serum Albumin Nanoparticles: Preparation, Characterization, and In Vitro Biological Studies

Lijun Zhang,[1,2,3] Junfeng Hui,[1,2,3] Pei Ma,[1,2,3] Yu Mi,[1,2,3] Daidi Fan,[1,2,3] Chenhui Zhu,[1,2,3] Lei Chi,[1,2,3] and Yanan Dong[1,2,3]

[1]*Shaanxi Key Laboratory of Degradable Biomedical Materials, School of Chemical Engineering, Northwest University, 229 North Taibai Road, Xi' an, Shaanxi 710069, China*
[2]*Shaanxi R&D Center of Biomaterials and Fermentation Engineering, School of Chemical Engineering, Northwest University, 229 North Taibai Road, Xi' an, Shaanxi 710069, China*
[3]*Biotech & Biomed Research Institute, Northwest University, 229 North Road Taibai, Xi' an, Shaanxi 710069, China*

Correspondence should be addressed to Yu Mi; mi_yu@nwu.edu.cn and Daidi Fan; fandaidi@nwu.edu.cn

Received 10 October 2018; Revised 11 December 2018; Accepted 2 January 2019; Published 27 March 2019

Guest Editor: Kakarla R. Reddy

Ginsenoside Rg3 (Rg3) is one of three triterpene saponins from red ginseng. It has important structural functions and pharmacological properties. However, due to its poor solubility, low bioavailability, and short half-life in blood circulation, its clinical application was unsuccessful for the treatment of a variety of cancers. In order to overcome this limitation, this study prepared mPEGylation-Rg3 bovine serum albumin nanoparticles (mPEG-Rg3-BSA NPs). The characteristics of the NPs, such as drug entrapment efficiency, drug loading efficiency, surface morphology, thermal stability, and cytotoxicity in vitro, were investigated. The results showed that the appropriate particle size of the obtained NPs was 149.5 nm, the water solubility and stability were better than free Rg3, and the drug entrapment efficiency and drug loading efficiency were 76.56% and 17.65%, respectively. Moreover, the cytotoxicity assays of the mPEG-Rg3-BSA NPs and free Rg3 revealed that the mPEG-Rg3-BSA NPs have greater anticancer effects in HepG2 cells and A549 cells. However, the cytotoxic effect of free Rg3 was higher than the mPEG-Rg3-BSA NPs in L929 cells. The results indicated that using the mPEGylation method and selecting BSA as a carrier to form the nanodrug carrier system were effective for improving the properties of Rg3.

1. Introduction

Cancer is a serious threat to human health and life and causes a high death rate [1]; there are various drugs available to cure cancer. However, their major drawbacks are poor distribution, poor water solubility, poor target specificity, and a short half-life in blood circulation, which reduces the therapeutic effect to a large extent. Therefore, clinical applications are unsuccessful for the treatment of a variety of cancers [2]. Ginsenoside is a sterol compound with three terpene saponins. It is mainly extracted from ginseng medicinal materials, including protopanaxadiols (Ppd) and protopanaxatriols (Ppt), which have many medicinal properties, such as anti-inflammatory, anticancer, and antioxidant effects [3]. 20(R)-Rg3 (Rg3) is one of the major Ppd types with no toxicity and has hydrophobic triterpenes, steroid aglycones, and hydrophilic sugar side chains in its structure. Recent studies showed that Rg3 is a powerful anticancer drug for the treatment of a variety of cancers [4]. It can inhibit the proliferation of tumor cells and induce the apoptosis of tumor cells. Moreover, it can prevent tumor cell adhesion, invasion, and metastasis and it can regulate the proliferation of tumor cells. Although Rg3 possesses a variety of medically beneficial effects, the clinical application of Rg3 is restricted due to its poor water solubility and short circulation half-life and bad target specificity into tumor tissues [5]. Furthermore, low aqueous solubility limits its bioavailability, thereby not distinguishing healthy from cancerous tissues [6]. It

requires polyethylene glycol (PEG) 400 or polyethoxylated castor oil and ethanol as a vehicle. These agents cause severe allergic reactions upon intravenous administration [7]. Polyethylene glycol modification is considered an ideal potential method for the delivery of poorly water-soluble drugs. Currently, it is one of the common techniques by which we can use it or its derivatives to improve the molecular structure of drugs. As a water-soluble restorative agent with the properties of nontoxicity and low immunity, it can increase the circulation half-life and colloidal stability under physiological salt concentrations [8, 9]. A number of small-molecule drugs, such as paclitaxel, camptothecin, and doxorubicin hydrochloride, have been modified by PEG or its derivatives [10, 11], and their solubility has been improved greatly. Therefore, we selected methoxy polyethylene glycol succinic acid (mPEG-SA) as a water-soluble restorative agent to enhance the water solubility of Rg3.

In recent years, great progress has been made in nanodrug delivery systems, which has been reported to accumulate drugs in tumor tissues more efficiently due to the enhanced permeability retention effect (EPR). They are designed to deliver poorly water-soluble drugs and improve the pharmacological and therapeutic properties of drugs administered parenterally. Moreover, the hydrophilicity of nanoparticles provides excellent water solubility and superior biocompatibility, because they effectively protect the activity of drugs, achieve slow and controlled release, and avoid reticuloendothelial system (RES) phagocytosis [12–14]. Thus far, many types of nanocarriers have been invented by researchers, such as lipid- or polymer-based nanoparticles, nanofibres, and biodegradable carrier systems [15–17]. As a common and natural biomacromolecule protein, studies show that BSA [18–20] has its own unique advantages with respect to drug delivery. Among them, BSA has been widely employed as a biomacromolecule nanocarrier for improving the therapeutic efficacy of anticancer drugs, which has important physiological functions in the body and regulates the total osmotic pressure of the blood. Furthermore, it has many advantages, such as being safe and nontoxic, with low immunogenicity, biodegradability, and good biocompatibility, and it is an abundant endogenous protein in human serum. Moreover, BSA NPs were prepared using the desolvation method followed by glutaraldehyde fixation [21]. Collectively, BSA can be considered a safe, effective, and biocompatible target carrier to deliver mPEG-Rg3 to form a nanodrug delivery system.

Briefly, this paper used mPEG-SA and BSA to improve the properties of Rg3, which were expected to enhance the aqueous solubility and exert anticancer effects by potent delivery of Rg3 with passive target specificity to tumor cells. As shown in Figure 1, Rg3 was modified by mPEG-SA to synthesize mPEG-Rg3, and then, mPEG-Rg3 was entrapped within the BSA to form mPEG-Rg3-BSA NPs using the desolvation method. The mPEG-Rg3-BSA nanostructure had characteristics of excellent stability, high anticancer effects, and slow release. Furthermore, the physicochemical and biochemical properties of mPEG-Rg3-BSA NPs were measured by dynamic light scattering (DLS), scanning electron microscopy (SEM), transmission electron microscopy (TEM), thermogravimetry (TG), and differential scanning calorimetry (DSC). The cellular uptake of mPEG-Rg3-BSA NPs was visualized using confocal laser scanning microscopy (CLSM), whereas the cytotoxicity of mPEG-Rg3-BSA NPs was evaluated by MTT assay, apoptosis was observed by chromatin staining with Hoechst 33342, and the in vivo biodistribution behavior was investigated by near-infrared imaging system.

2. Materials and Methods

2.1. Materials. BSA was obtained from AMRESCO (Solon, OH, USA). Ginsenoside Rg3 was purchased from Sigma-Aldrich (Shanghai, China). Methoxy polyethylene glycol succinic acid (mPEG-SA) was purchased from Hua Teng Pharma. Co. Ltd. (Hunan, China). Dicyclohexylcarbodiimide (DCC), Dimethylaminopyridine (DMAP). and N,N-Dimethylformamide (DMF) were purchased from Tianjin KGM Chemical Reagent Co. Ltd. (Tianjin, China). Ultrapure water used in all experiments was produced with a Milli-Q synthesis system (Millipore Corp., Billerica, MA, USA). Fluorescein isothiocyanate (FITC) was purchased from Sigma (USA), and Gibco Dulbecco's modified Eagle's medium (DMEM) was obtained from HyClone (LA, USA). Foetal bovine serum (FBS) was supplied by Gibco (NY, USA). Penicillin, streptomycin, and methyl thiazolyl tetrazolium kit (MTT) were supplied by KeyGEN Biological Technology Development Co. Ltd. (Nanjing, China). Hoechst 33342 fluorescent dye was obtained from Beyotime Biotechnology (Shanghai, China). DiR was purchased from Biotium Inc. (USA). The human hepatoma carcinoma cells (HepG2 cells) and human lung carcinoma cells (A549 cells) were obtained from the American Type Culture Collection (ATCC) (Manassas, VA, USA). All other regents were of analytical grade.

2.2. Synthesis of mPEG-Rg3. mPEG-Rg3 was prepared by esterification [11]. As shown in Figure 2(a), mPEG-SA (190 mg, 0.095 mmoL) was activated by DMAP (3.863 mg, 0.317 mmoL) and DCC (19.58 mg, 0.095 mmoL) in a solution (4 mL DMF and 1 mL CH_2Cl_2) after the solution was stirred for 0.5 h at room temperature. Then, Rg3 (25 mg, 0.032 mmoL) was added to the mixture. When the solution was stirred for 72 h at room temperature, the prepared compounds were extracted three times using ultrapure water and dichloromethane and then evaporated in vacuo. At the same time, it was further purified on a silica gel column, after which the products were dialyzed for 72 h against purified water. The mPEG-Rg3 was obtained by freeze drying. Then, the structure of mPEG-Rg3 was confirmed by ^{13}C NMR (Japan Electron Optics Laboratory Co. Ltd., Japan) and FT-IR (Brook Spectrometer Co. Ltd., USA).

2.3. Preparation of mPEG-Rg3-BSA NPs. The mPEG-Rg3-BSA NPs were prepared using a desolvation technique [22–24]. As shown in Figure 2(b), BSA (2 mL, 10 mg/mL) was first dissolved in ultrapure water; then, NaOH solution (30 μL, 0.02 mg/mL) was slowly added to the BSA solution. The mPEG-Rg3 (6 mL, 0.76 mg/mL) was dissolved in absolute ethyl alcohol and later added slowly to the BSA solution.

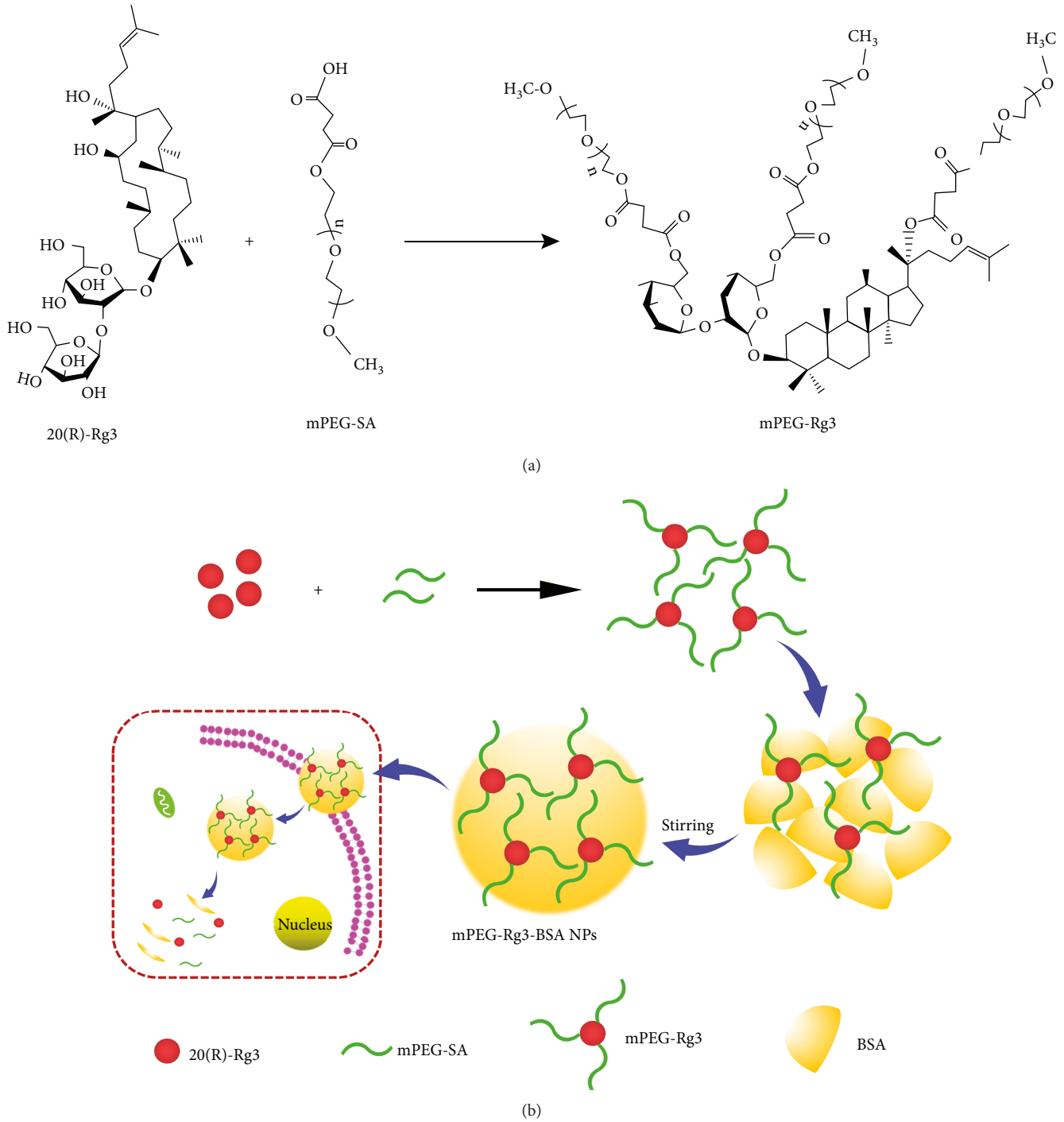

Figure 1: Schematic illustration of the synthesis of mPEG-Rg3 (a) and mPEG-Rg3-BSA NPs (b).

After the reaction mixture was stirred at 500 rpm for 24 h at room temperature, this reconstitution solution was centrifuged (18000 × g, 15 min) to separate the unloaded Rg3. This purification process was repeated six times using ultrapure water. After each centrifugation, the residue was redispersed to the original volume with deionized water using a mechanical stirrer. Then, the resulting solution was freeze dried after a final redispersion to achieve mPEG-Rg3-BSA NPs. Furthermore, the supernatants from each centrifugation were pooled to determine the drug loading capacities (DLC) and encapsulation efficiency (EE).

2.4. Characterization of mPEG-Rg3-BSA NPs. The characterization of mPEG-Rg3-BSA NPs was confirmed by FT-IR. The mPEG-Rg3-BSA NP suspension was diluted with water, and the average size and distribution of mPEG-Rg3-BSA NPs were determined by DLS (Malvern Instruments Ltd., UK) at room temperature. The size and morphology of the nanoparticles

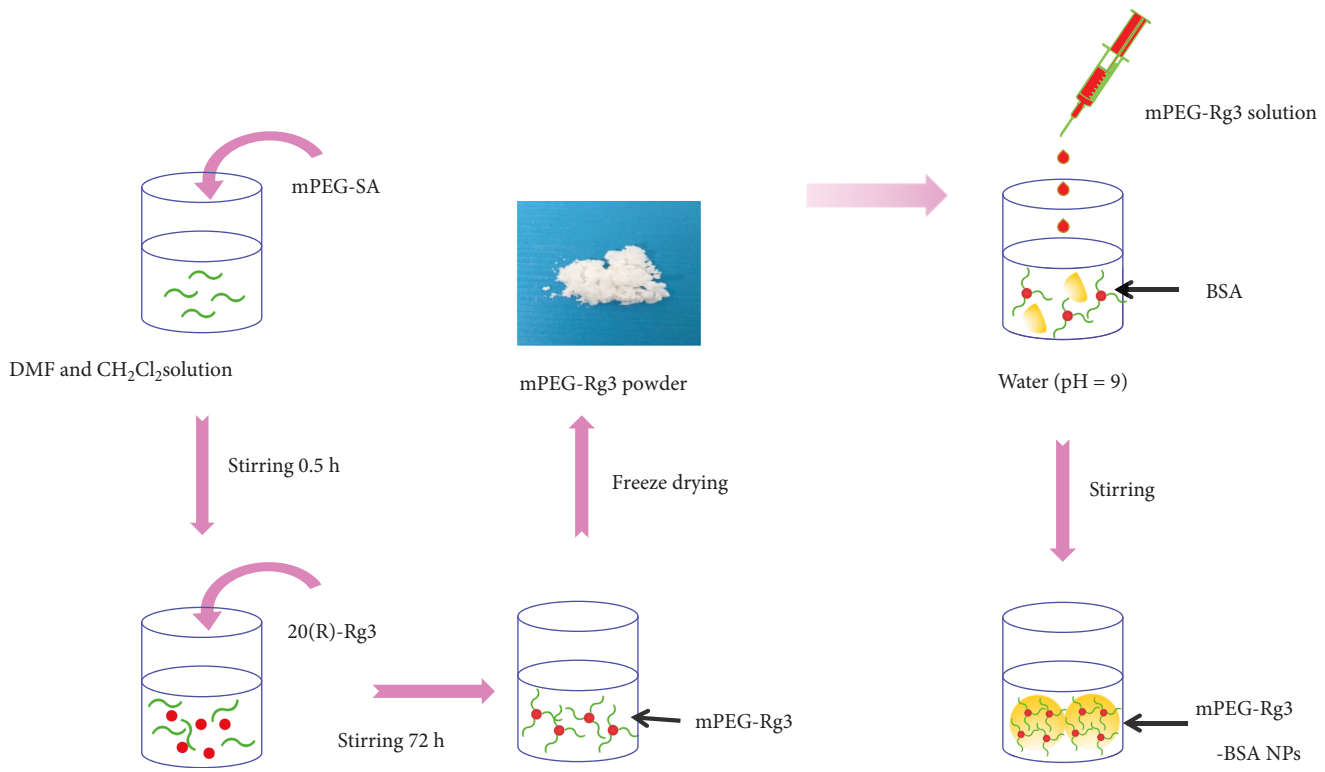

Figure 2: Synthetic route for the preparation of mPEG-Rg3 (a) and mPEG-Rg3-Rg3 NPs (b).

were observed using SEM (Hitachi Ltd., Japan) and TEM (Hitachi Ltd., Japan). For SEM, the mPEG-Rg3-BSA NP powder was placed on a conductive tape and the excess powder was removed with tweezers. Because of the poor conductivity of the sample, gold plating was needed. After an interval, the mPEG-Rg3-BSA NP powder was deposited on the sample plate by SEM. For TEM, the proper amount of mPEG-Rg3-BSA NP suspension was absorbed and the suspension was first removed to a special copper screen. It was incubated for five minutes, and filter paper was used to dry the redundant suspension in the copper screen. For negative staining with 3% phosphotungstic acid solution, the suspension was stained for 3 min. After staining, the morphology and size of the mPEG-Rg3-BSA NPs were investigated by TEM.

The supernatant from each centrifugation was collected to determine the drug entrapment efficiency and drug loading efficiency, which was analyzed for residual drug concentration using high-performance liquid chromatography (HPLC) (Rg3: 203 nm; specific volume ratio mixture of acetonitrile-water as a mobile phase; flow rate at 1.5 mL·min^{-1}) [25, 26]. DLC and EE were calculated according to the following equations:

$$\begin{aligned} \mathrm{DLC}(\%) &= \left(\frac{\text{weight of loaded drug}}{\text{weight of nanoparticles}}\right) \times 100\%, \\ \mathrm{EE}(\%) &= \left(\frac{\text{weight of loaded drug}}{\text{weight of drug of Rg3}}\right) \times 100\%. \end{aligned} \quad (1)$$

The thermal properties of Rg3, mPEG-Rg3, BSA, and mPEG-Rg3-BSA NPs were investigated using TG and DSC (Shimadzu, Kyoto, Japan). For TG, the samples were set from 50°C to 750°C at a ramping rate of 10°C·min^{-1}; 20 mg of each sample was placed in a standard aluminum pan. For DSC, the samples were set from 30°C to 550°C at a ramping rate of 10°C·min^{-1}; 20 mg of each sample was placed in a standard aluminum pan.

For the time-dependent stability studies, the sizes and zeta potentials were measured by evaluating the time dependency of mPEG-Rg3-BSA NPs at regular time intervals. Moreover, the mPEG-Rg3-BSA NPs were studied for up to 18 days at 4°C [27].

The release of drugs from the NPs was analyzed using a dialysis method [28]. The mPEG-Rg3-BSA NP suspension was first loaded into a dialysis bag (MWCO 3500). Then, the dialysis bag was immersed in 80 mL of PBS (pH = 7.4) and placed in a shaking bath (37°C, 100 rpm). An aliquot (2 mL) of the medium was collected at timed intervals, and the Rg3 concentration in the buffer was determined using HPLC. The amount released was then calculated. Each profile represents the average of three independent runs with the same sampling schedules, and the standard deviation of each point was typically 5% or less.

2.5. Haemolysis Assay. Haemolysis experiments were conducted to evaluate the biocompatibility of free Rg3 and mPEG-Rg3-BSA NPs according to the general procedure of the haemolysis test. Five millilitres of fresh blood samples was collected from rabbits and then added to blood collection tubes immediately to prevent coagulation. One millilitre of fresh blood samples from the blood collection tube was placed into 1.25 mL normal saline, and the different

concentrations free Rg3 and mPEG-Rg3-BSA NP suspension (5 mL) were dispersed in 100 μL aliquots. At the same time, normal saline and distilled water were dispersed in 100 μL aliquots as negative and positive controls. Then, samples were incubated under constant shaking for 1 h at 37°C. The red blood cells (RBCs) were collected by centrifugation at 1500 rpm for 5 min at 4°C. After centrifugation at 1500 rpm for 5 min at 4°C, the supernatant (100 μL, 96-well plates) was analyzed for haemoglobin release at 545 nm using a microplate spectrophotometer (Tecan, Switzerland) [29]. Haemolysis was determined from three independent experiments. The haemolytic ratio (HR) was calculated according to the following equation:

$$\mathrm{HR}\% = \frac{A_{\text{sample}} - A_{\text{negative control}}}{A_{\text{positive control}} - A_{\text{negative control}}} \times 100\%. \quad (2)$$

2.6. In Vitro Cell Cytotoxicity and Cellular Uptake. The MTT assay was used to evaluate the cell inhibition of different samples [30, 31]. Briefly, L929 cells and HepG2 cells and A549 cells were seeded in 96-well plates at a density of 1×10^4 per well in 100 μL culture medium and incubated for 24 h. Then, the cells were treated with samples at 37°C in a humidified incubator with 5% CO_2 for 24 h. The free Rg3 and mPEG-Rg3-BSA NPs (60, 120, 180, 240, and 300 μM) were dissolved in dimethyl sulfoxide and diluted in culture medium before the assay. A total of 50 μL of MTT solution was added to each well and incubated for 2 h at 37°C. Then, the supernatants were removed and added to 150 μL of DMSO. The absorbance at 490 nm was then read with a microplate reader (BioTek Instruments Inc., USA). The data were representative of three independent experiments.

Cellular uptake and distribution of Rg3 from the NPs were observed by CLSM (Leica, Germany) [32]. First, mPEG-Rg3-BSA NPs (180 μM) were labelled with FITC to investigate the uptake of NPs into L929 and HepG2 cells according to the method of Leamon and Low (1991). After the L929 and HepG2 cells achieved 70–80% confluency, the cells were trypsinized and seeded onto culture slides at a density of 7×10^5 cells per well (surface area of 10 cm^2 per well) and incubated for 24 h at 37°C. FITC-labelled mPEG-Rg3-BSA NPs were added and incubated for 4 h. After incubation, all reagents were removed. Cells were washed with PBS (pH = 7.4) at least 3 times for 2 minutes each and fixed with paraformaldehyde for 10 min. After the cells were washed with PBS, the nuclei were counterstained with DAPI for 5 min. Finally, the cell monolayer was washed three times with PBS and observed by CLSM.

2.7. Apoptosis Assay. Apoptosis was observed by chromatin staining with Hoechst 33342. HepG2 cells were seeded in 96-wells and incubated for 24 h at 37°C. The mPEG-Rg3-BSA NPs and free Rg3 (180, 240, and 300 μM) were added and incubated for 24 h. After incubation, all reagents were removed. Cells were washed with RPMI 1640 cell culture medium at least 2 times for 2 minutes each. Then, Hoechst 33342 (100 μL) was added in the dark. When cells were incubated for 15 min, they were washed with PBS at least 3 times. The nuclear morphology changes were observed under a fluorescence microscope (Nikon, Tokyo, Japan) [33].

2.8. Biodistribution of DiR-Loaded mPEG-Rg3-BSA NPs in Tumor-Bearing Mice. To study the biodistribution of the mPEG-Rg3-BSA NPs in tumor-bearing mice [34], the mPEG-Rg3-BSA NPs were labelled with DiR using the same protocol for the preparation of the mPEG-Rg3-BSA NPs. When the subcutaneous HepG2 tumors grew up to 300~400 mm^3, mice were injected with free DiR and DiR-labelled mPEG-Rg3-BSA NPs at a dose of 0.5 mg/kg. Fluorescent images were taken at different intervals (2, 8, and 24 h) using the vivo imaging system (IVIS® Lumina XR Series III, PerkinElmer). Then, the HepG2 tumor-bearing mice were dissected at 24 h for imaging.

2.9. Statistical Analysis. All data are given as the mean values ± standard deviation (SD). A p value of 0.05 or less was considered to be statistically significant.

3. Results and Discussion

3.1. ^{13}C NMR and FT-IR of mPEG-Rg3-BSA NPs. The mPEG-Rg3 powder was obtained by freeze drying, and the water solubility of Rg3 was 1 mg/mL after being conjugated with mPEG-SA, and the yield was 48.5%. As shown in Figure 3(a), a characteristic succinic acid peak of mPEG-SA was present at 174.48 ppm. For the next step, mPEG-SA was conjugated to Rg3 via the formation of ester bonds. As expected, the ^{13}C NMR spectrum of the mPEG-Rg3 conjugate contains all expected resonance peak characteristics of mPEG-SA and Rg3 and the carbon double bonds of mPEG-Rg3 were at 124.12 ppm and 129.90 ppm. The extent of mPEG-SA conjugation was calculated based on the ester bonds of mPEG-Rg3 at 172.18 ppm and 169.38 ppm. From the ^{13}C NMR results, we determined that the C-20 hydroxyl and C-6 sugar hydroxyl groups of Rg3 underwent ester bonding [33].

As shown in Figure 3(b), the mPEG-Rg3 contained the characteristic peak ($\nu_{C=C}$) of Rg3 at 1647 cm^{-1} and the wavelength $C = O$ was at 1734 cm^{-1}. From the FT-IR, Rg3 may react with the carboxylic group of mPEG-SA. Moreover, this conclusion tested the results of Figure 3(a). At the same time, the FT-IR results demonstrated that the characteristic peak of carbon oxygen bonds (ν_{C-O}, 1075 cm^{-1}) for mPEG-Rg3 appeared for mPEG-Rg3-BSA NPs, which was possible because the hydroxyl of Rg3 interacted with the aromatic residues (tryptophan, tyrosine) of BSA [34], and Rg3 was encapsulated into the core of the NPs.

3.2. Size and Morphology of mPEG-Rg3-BSA NPs. The desolvation technique [35], which is classic, simple, and easy to operate, was used to prepare the mPEG-Rg3-BSA NPs. The results demonstrated that the ratio of solvent and the pH of the BSA solution were important to avoid coalescence and agglomeration during desolvation. For the pH of the BSA solution, changes in pH can lead to denaturation and had an effect on the charge of the raw materials, as lower pH values (such as pH 7 or 8) would lead to precipitation and higher pH values (pH = 10) would increase the size of the

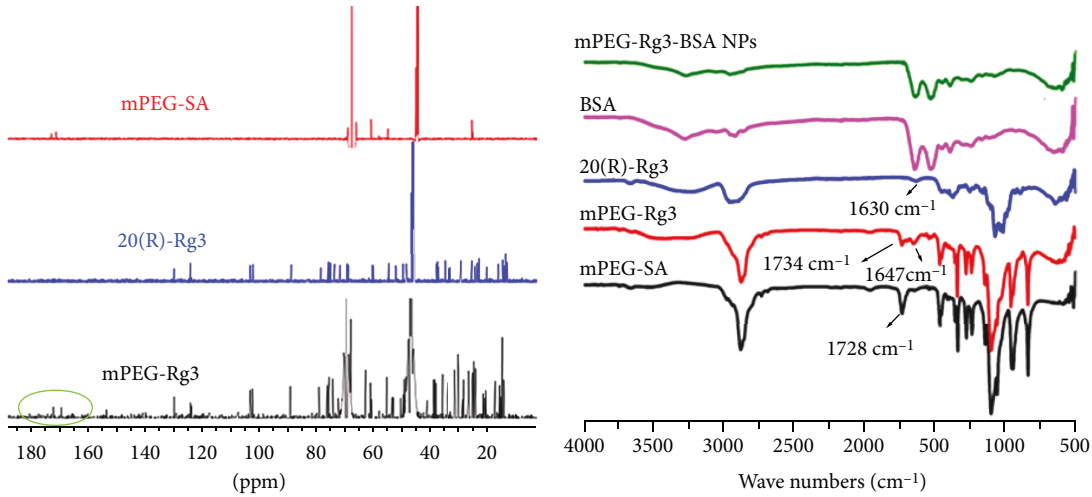

FIGURE 3: (a) The ^{13}C NMR spectrum of mPEG-Rg3, 20(R)-Rg3, and mPEG-SA. (b) The FT-IR spectra of mPEG-SA, mPEG-Rg3, 20(R)-Rg3, BSA, and mPEG-Rg3-BSA NPs.

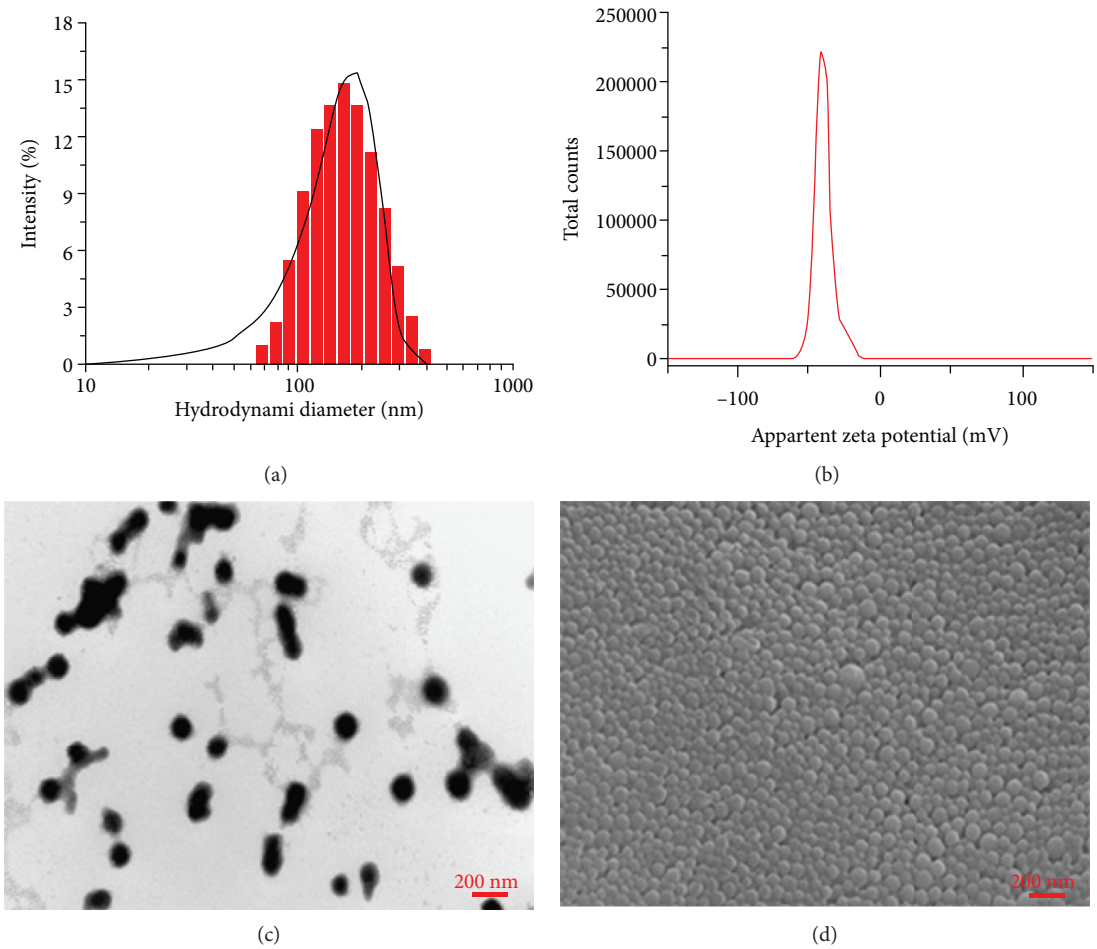

FIGURE 4: (a) Hydrodynamic size distribution, (b) zeta potential, (c) TEM images, and (d) SEM images of mPEG-Rg3-BSA NPs.

NPs, so the optimum pH was determined to be pH 9. As shown in Figure 4, the NP images and size distribution were measured by DLS and electron microscopy. Imaging showed that the NPs were generally spherical in shape with a narrow size distribution and that the mean particle size and zeta potential of the mPEG-Rg3-BSA NPs were 149.5 nm

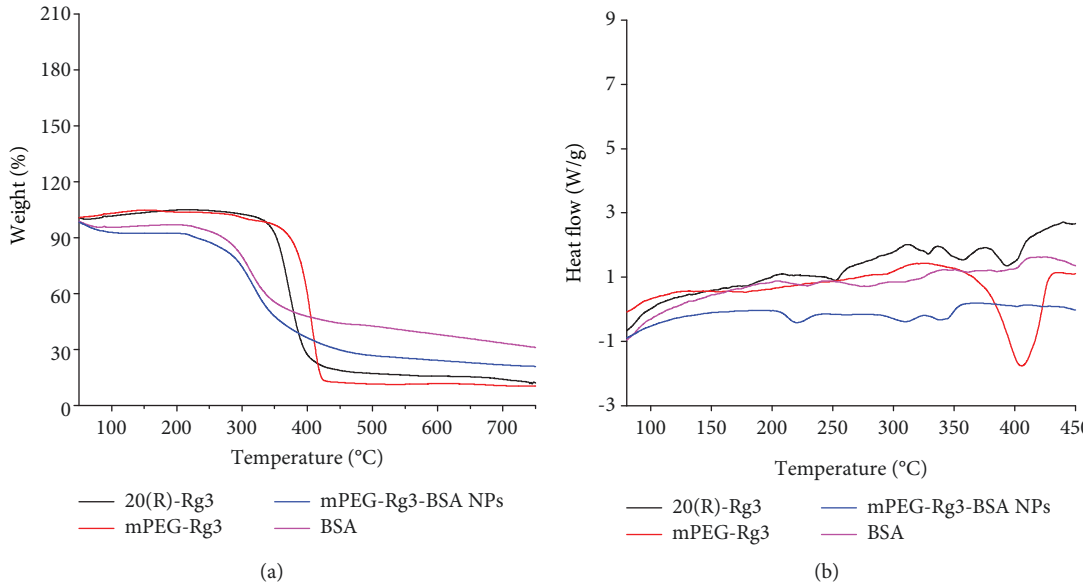

Figure 5: (a) TG analysis curves and (b) DSC thermograms of BSA, mPEG-Rg3-BSA NPs, mPEG-Rg3, and 20(R)-Rg3.

(PDI = 0.117) and -40.2 mV, respectively. The higher the zeta potential, the more stable the NPs. In addition, when the particle size is less than 200 nm, nanoparticles are more likely to enter cells by EPR, and moreover, the size was reported to more efficiently resist capture by RES. The mean drug loading capacity of the mPEG-Rg3-BSA NPs was 17.65%, and the EE value of Rg3 for the mPEG-Rg3-BSA NPs was 76.56%. At the loading level of mPEG-Rg3-BSA NPs, the effective concentration of Rg3 was 6.8 mg/mL, which is 107 times higher than the intrinsic water solubility of free Rg3 (0.063 mg/mL).

3.3. TG and DSC Study. TG is used to analyze the relationship between the quality of sample and temperature change [36]. It can describe the thermal stability of NPs. As shown in Figure 5(a), the results depicted a slower degradation rate of the mPEG-Rg3-BSA NPs, indicating its improved stability compared to Rg3. The curves of Rg3 and mPEG-Rg3 had no significant difference, which showed the degradation of Rg3 and mPEG-Rg3 with respect to increasing temperature. Meanwhile, BSA and mPEG-Rg3-BSA NPs began to lose weight from 50°C to 200°C, which was attributed to water loss. When the temperature was 240°C, abrupt decrease in weight loss happened, which may be due to the loss of small molecules such as ammonia and carbon dioxide. For mPEG-Rg3-BSA NPs, the total ratio of weight loss was about 79.4%. It exhibited a higher weight loss, lower than that for BSA, which is consistent with an increase in organic content of the nanoparticles upon loading of Rg3. Moreover, the results also suggested that the stability of NPs was better than that of Rg3 and the products were successfully degraded at higher temperatures.

DSC is used to evaluate the status of the drug in the drug delivery system and to investigate the potential change of drug properties [37]. As shown in Figure 5(b), the Rg3 powder showed a significant sharp melting peak at 406.21°C, which was also recorded in the mPEG-Rg3 powder. Meanwhile, according to the TG curve, the peak indicated the crystalline state of Rg3. However, the peak disappeared in the thermogram of mPEG-Rg3-BSA NPs, revealing that Rg3 was not in the crystalline state after its presence in the nanoparticles, in accordance with the TG results. In addition, this result indicated that the obtained nanodrug delivery system was stable.

3.4. In Vitro Stability Study. Stability [38] is a very important factor that contributes to the accumulation of NPs at tumor sites. Whether nanoparticles were stable at the nanoscale is key for them to exhibit unique properties. The time-dependent stability of mPEG-Rg3-BSA NPs was determined using the particle size and zeta potential analysis, with respect to different time intervals over 18 days. As shown in Figure 6, there was no significant change in the size and zeta potential of mPEG-Rg3-BSA NPs at 37°C. The size and zeta potential fluctuated at approximately 165 nm and -35 mV, respectively. The results suggested that the stability of mPEG-Rg3-BSA NPs occurred for 18 days in an aqueous system at 37°C.

3.5. In Vitro Drug Release of mPEG-Rg3-BSA NPs. Drug release [39] from nanosized formulations determines the pharmacokinetic properties of a drug in the body after intravenous injection. A sustained drug release pattern is desirable for an injection formulation because of increased systemic exposure, enhanced therapeutic efficacy, and decreased dosing frequency. As shown in Figure 7, the release pattern of Rg3 from NPs was investigated in an in vitro model for 7 days. The initial fast release stage and slow release stage attributed to the continuous degradation of the BSA. The results confirmed that nanodrug delivery system can release

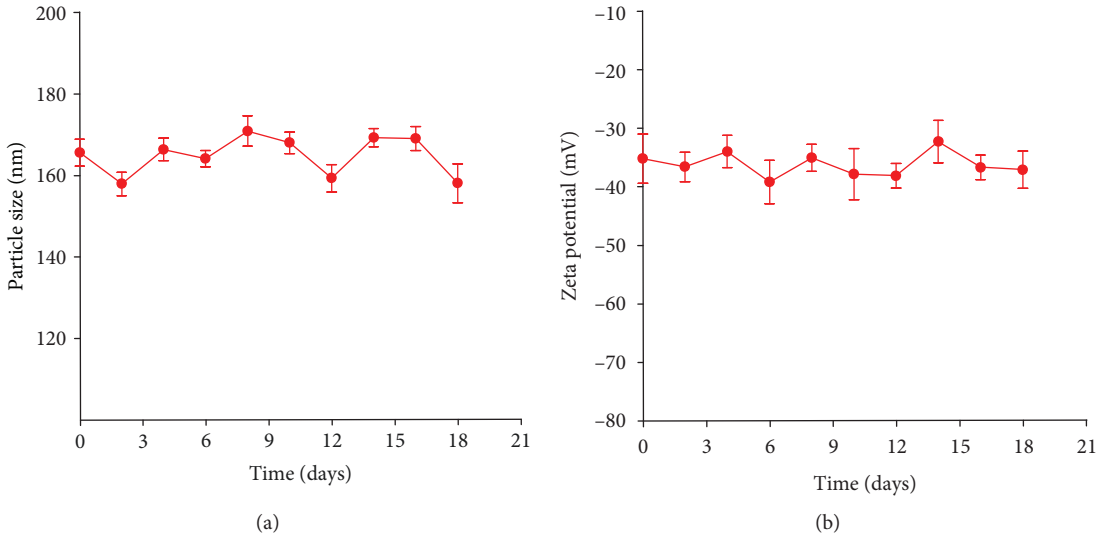

Figure 6: In vitro stability of mPEG-Rg3-BSA NPs at 37°C using particle size analysis (a) and zeta potential analysis (b), with respect to different time intervals. Values are reported as the mean ± SD for triplicate samples.

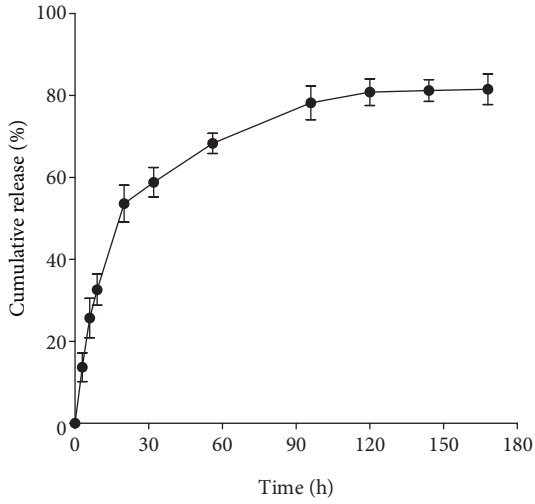

Figure 7: The ginsenoside Rg3 release kinetics from the mPEG-Rg3-BSA NPs in buffer at pH 7.4 and 37°C. Values are reported as the mean ± SD for triplicate samples.

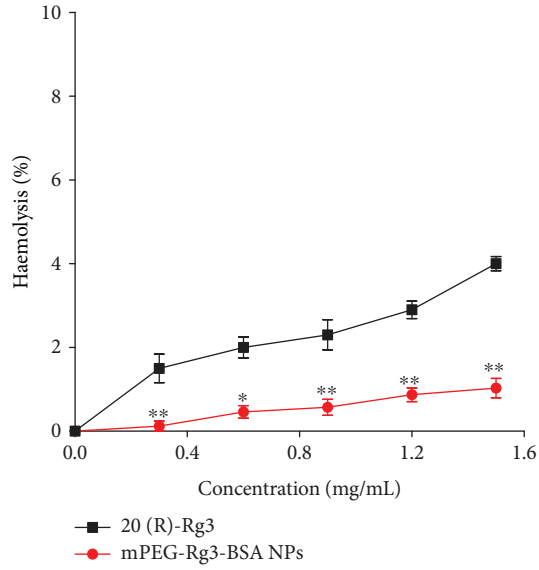

Figure 8: In vitro haemolysis assay of 20(R)-Rg3 and mPEG-Rg3-BSA NPs compared to ultrapure water and physiological saline measured at 545 nm. Values are reported as the mean ± SD for triplicate samples. ∗ represents $p < 0.05$; ∗∗ represents $p < 0.01$.

slowly. Meanwhile, the cumulative release was 59.7% and 85.8% at 32 h and 120 h, respectively. Moreover, the decrease of irregular release behavior may be achieved by long circulation time, thereby enhancing the bioavailability and reducing the cytotoxicity in normal tissues.

3.6. Haemolysis Study. Biocompatibility is a vital factor for in vivo bioapplications [40]. Haemolysis is an important index to evaluate the biocompatibility of nanocarriers, and the quantitative measurement of the haemoglobin released provides an indication of the potential damage to RBCs. In general, drug carriers can be administered by intravenous injection when the haemolysis ratio is less than 5%. As shown in Figure 8, the haemolysis percentages of free Rg3 and mPEG-Rg3-BSA NPs from 0.3 to 1.5 mg/mL were less than 5%. Moreover, the haemolysis of free Rg3 was much higher than those of mPEG-Rg3-BSA NPs, further confirming the safety of mPEG-Rg3-BSA NPs for intravenous injection. This was possibly due to the antihaemolytic properties of the raw material. Collectively, it was concluded that NPs were a kind of a safe tumor drug carrier.

3.7. In Vitro Cell Cytotoxicity. The cytotoxicity of mPEG-Rg3-BSA NPs and free Rg3 to HepG2 and A549 cells was determined by MTT assay [41] to assess the drug delivery efficiency and determine the cell inhibition rate and antiactivity in vitro. The cell inhibition rate was measured at 24 h,

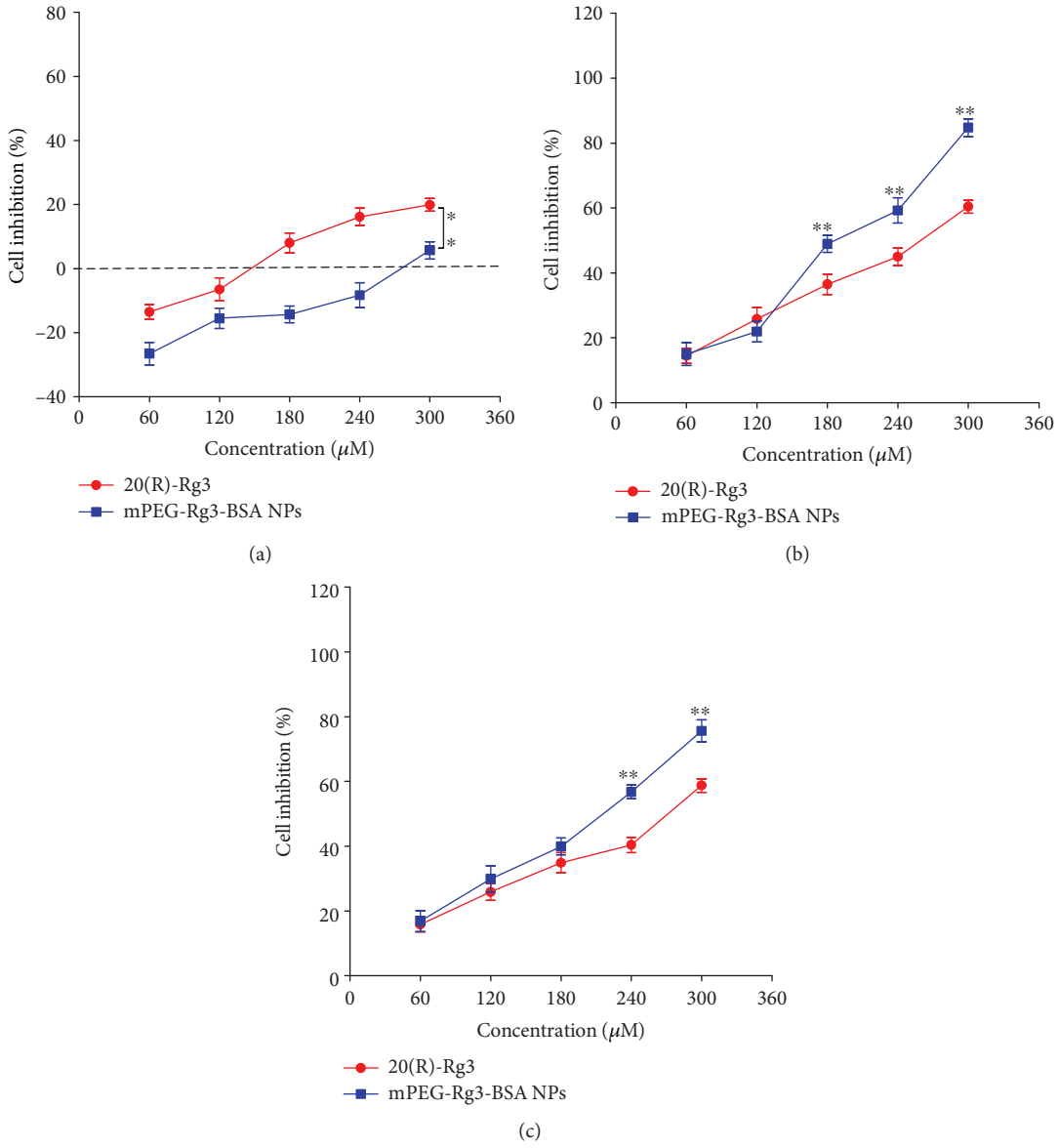

Figure 9: The cell viability of L929 cells (a) and HepG2 cells (b) and A549 cells (c) treated for 24 h measured using an MTT assay. Values are reported as the mean ± SD for triplicate samples. ∗ represents $p < 0.05$.

and the concentration of all samples was calculated based on the amount of Rg3 present in the nanoparticles. As shown in Figure 9(a), for the L929 cells, the inhibition rate of the free Rg3 and mPEG-Rg3-BSA NPs was increased with increasing Rg3 drug concentrations but mPEG-Rg3-BSA NPs more promoted cell proliferation than free Rg3 at 60~120 μM. As shown in Figure 9(b), for the HepG2 cells, the inhibition rate of the mPEG-Rg3-BSA NPs was increased with increasing drug concentrations and the cell cytotoxicity of mPEG-Rg3-BSA NPs was higher than that of free Rg3 at the same concentration. When the concentration of drug was 240 μM, the inhibition rates of the mPEG-Rg3-BSA NPs and free Rg3 were 59.20% and 40.08%, respectively, and the IC_{50} values of the mPEG-Rg3-BSA NP- and free Rg3-treated HepG2 cells were 195.3 μM and 252.88 μM, respectively. As shown in Figure 9(b), for the A549 cells, there was similar anticancer effect between mPEG-Rg3-BSANPs and free Rg3 at 24 h at the same concentration of Rg3. When the concentration of drug was 240 μM, the inhibition rates of the mPEG-Rg3-BSA NPs and free Rg3 were 56.75% and 40.38%, respectively, and the IC_{50} values of the mPEG-Rg3-BSA NP- and free Rg3-treated HepG2 cells were 207.51 μM and 266.76 μM, respectively. As a whole, the cell inhibition rate of HepG2 cells was higher than that of the A549 cells at 24 h. Therefore, these results suggested that our fabricated mPEG-Rg3-BSA NPs could be an efficient drug carrier for the targeted cancer therapy of HepG2 cells and the cytotoxicity of mPEG-Rg3-BSA NPs was higher than that of free Rg3 to cancer cells. Collectively, the nanodrug delivery system enhanced the anticancer activity of drug to cancer cells and decreased the cytotoxicity of Rg3 to normal cells.

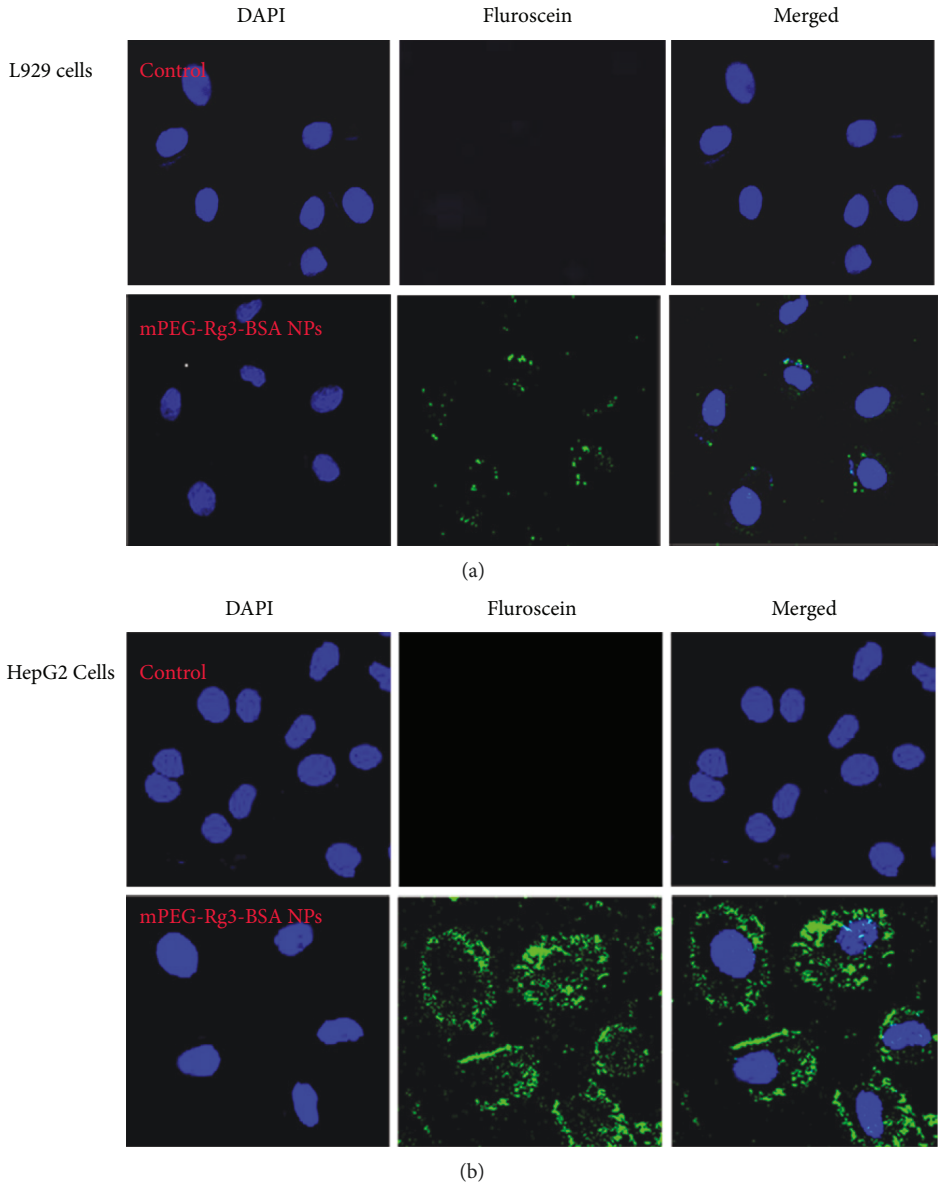

Figure 10: mPEG-Rg3-BSA NP uptake by cultured L929 and HepG2 cells. L929 and HepG2 cell monolayers were incubated with cell culture medium (control) and FITC-labelled nanoparticles (180 μM) for 4 h at 37°C. Magnification is ×800.

3.8. Cellular Uptake Assay. In general, free drug molecules entered the cytoplasm of the cell by passive diffusion. However, NPs were taken up by cells through an endocytic pathway and endocytic delivery using nanoparticles maintains a higher concentration in the cytoplasm for nanoparticles comparing with free drug. To study the effective drug delivery of NPs, L929 and HepG2 cell monolayers were incubated with FITC-labelled nanoparticles [42]. When the concentration of mPEG-Rg3-BSA NPs was 180 μM, the cell-associated fluorescence was evaluated using a fluorescence spectrophotometer. As shown in Figure 10, the green image demonstrated that the FITC-labelled mPEG-Rg3-BSANPs entered the cytoplasm of L929 cells and HepG2 cells and HepG2 cells contained higher fluorescence intensity than L929 cells. The results confirmed that nanoparticles were more efficiently taken up by tumor cells. In addition, the images also revealed the anticancer effect and apoptosis of cancer cells caused by mPEG-Rg3-BSA NPs.

3.9. Apoptosis Assay. HepG2 cell apoptosis caused by mPEG-Rg3-BSA NPs and free Rg3 was characterized by Hoechst 33342 staining [43]. In general, morphological changes, such as cell shrinkage and condensed and fragmented chromatin, are associated with apoptotic cell death. As shown in Figure 11, the Hoechst 33342 staining results were obtained using fluorescence microscopy and the control cells did not show any apoptotic bodies. Cells that were treated with increasing concentrations of mPEG-Rg3-BSA NPs and free Rg3 showed a progressive accumulation of condensed and fragmented chromatin. Furthermore, when the concentration of Rg3 was 300 μM, the apoptosis rate caused by mPEG-Rg3-BSA NPs was much higher than that by the free

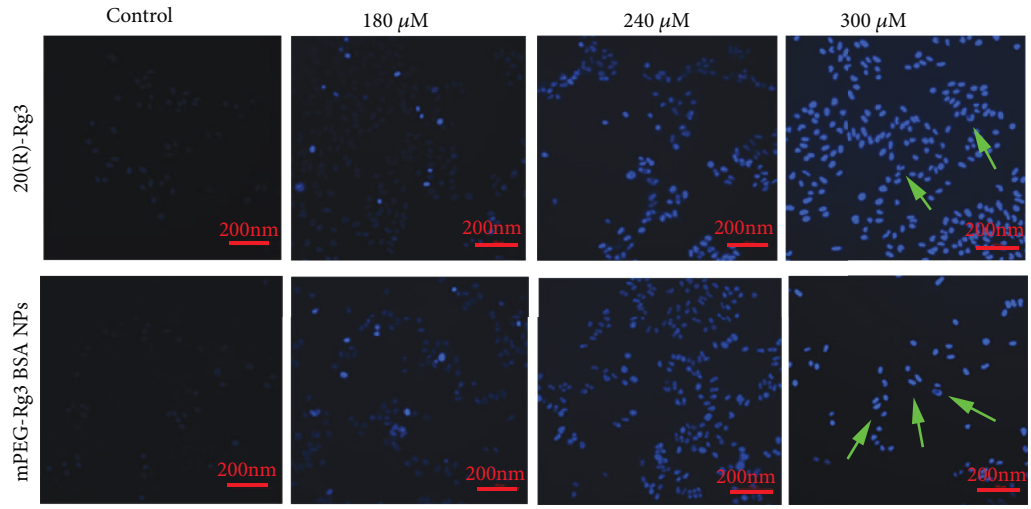

Figure 11: Apoptosis of HepG2 cells from 20(R)-Rg3 and mPEG-Rg3-BSA NPs evaluated by Hoechst 33342 staining. Magnification is ×100.

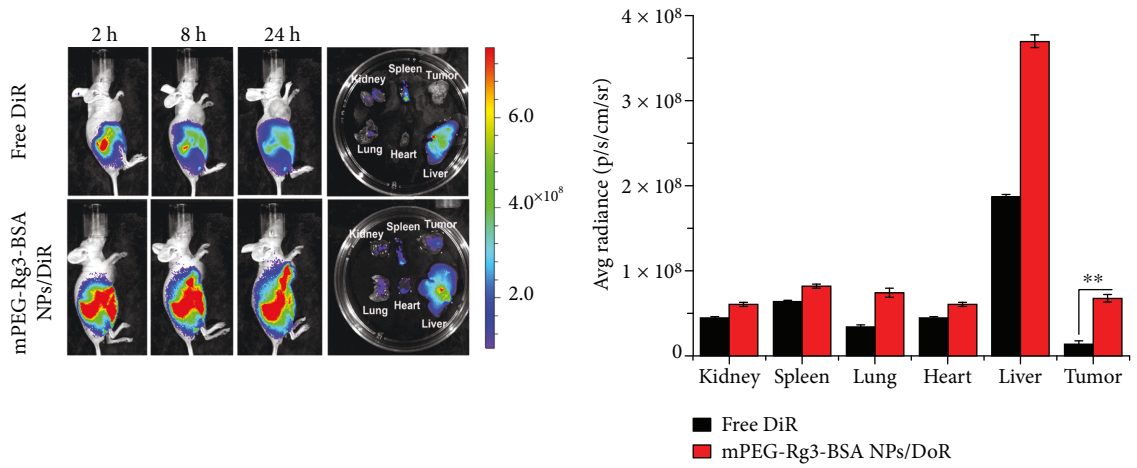

(a) (b)

Figure 12: (a) In vivo whole-animal imaging of mice bearing subcutaneous HepG2 tumors treated with free DiR and mPEG-Rg3-BSA NPs/DiR with different formulations at 2 h, 8 h, and 24 h and ex vivo fluorescence imaging of dissected organs after 24 h postinjection; (b) quantitative analysis of the fluorescence intensity of DiR in tumor tissue examined using the in vivo imaging system. Values are reported as the mean ± SD for triplicate samples. ∗∗ represents $p < 0.01$.

Rg3, and for the mPEG-Rg3-BSA NPs, the number of nuclei decreased. This demonstrated the apoptotic mechanism of cell death that occurred in cancer cells after exposure to mPEG-Rg3-BSA NPs and free Rg3. Moreover, the results also showed that the cytotoxicity for mPEG-Rg3-BSA NPs to cancer cells was higher than free Rg3.

3.10. Biodistribution of DiR-Loaded mPEG-Rg3-BSA NPs in Tumor-Bearing Mice. To estimate the in vivo biodistribution behavior of the mPEG-Rg3-BSA NPs, free DiR and DiR-labelled mPEG-Rg3-BSA NPs were injected into tumor-bearing mice. As shown in Figure 12, in the DiR-labelled mPEG-Rg3-BSA NP group, the fluorescence of DiR in the body of the mouse remained throughout the full experiment. However, the fluorescence of DiR quickly declined from 8 h postinjection for the free DiR group. Results confirmed that the fluorescence intensity appeared at the tumor site and was increasing as the time passes. DiR-labelled mPEG-Rg3-BSA NPs exhibited better accumulation than the free DiR group in the tumor; the fluorescence intensity at the tumor site was 5.4-fold higher than that of free DiR. Thus, we concluded that the hydrophilic corona preferable passive targeting ability of the NPs could significantly prolong drug blood circulation, which was beneficial for the mPEG-Rg3-BSA NPs to achieve an EPR effect.

4. Conclusions

In conclusion, this study used the mPEGylation method and selected BSA as the nanocarrier to prepare the nanodrug delivery system. This nanodrug delivery system improved the property of Rg3 and exhibited several attractive properties,

including good slow-release properties, good stability, the low cytotoxicity to the normal cells, and the selective ability to tumor cells. Furthermore, the mPEG-Rg3-BSA NPs enhanced the therapeutic effects compared to free Rg3. Therefore, it was a promising nanodrug delivery system for cancer therapy and the solubility and therapeutic effect of Rg3 could be better employed for future therapeutic applications by loading it in a BSA nanocarrier.

Data Availability

The data used to support the findings of this study are include within the article, which permits unrestricted use, distribution, and reproduction in any medium, provided that the original work is properly cited.

Conflicts of Interest

The authors declared no potential conflicts of interest with respect to the research, authorship, and/or publication of this article.

Acknowledgments

This study was financially supported by the National Natural Science Foundation of China (21676214, 21676215), Shaanxi Key Laboratory of Degradable Biomedical Materials Program (2014SZS07-K04, 2014SZS07-P05, js103, 2014SZS07-Z01, 2014SZS07-Z02, 2015SZSj-42, 2016SZSj-35, and 2014SZS07-K03), and Shaanxi R&D Center of Biomaterials and Fermentation Engineering Program (2015HBGC-04).

References

[1] T. T. Zuo, R. S. Zheng, H. M. Zeng, S. W. Zhang, and W. Q. Chen, "Female breast cancer incidence and mortality in China, 2013," *Thoracic Cancer*, vol. 8, no. 3, pp. 214–218, 2017.

[2] A. Stornetta, M. Zimmermann, G. D. Cimino, P. T. Henderson, and S. J. Sturla, "DNA adducts from anticancer drugs as candidate predictive markers for precision medicine," *Chemical Research in Toxicology*, vol. 30, no. 1, pp. 388–409, 2017.

[3] J. Upadhyaya, M. J. Kim, Y. H. Kim, S. R. Ko, H. W. Park, and M. K. Kim, "Enzymatic formation of compound-K from ginsenoside Rb1 by enzyme preparation from cultured mycelia of *Armillaria mellea*," *Journal of Ginseng Research*, vol. 40, no. 2, pp. 105–112, 2016.

[4] X. Zheng, W. Chen, H. Hou et al., "Ginsenoside 20(S)-Rg3 induced autophagy to inhibit migration and invasion of ovarian cancer," *Biomedicine & Pharmacotherapy*, vol. 85, pp. 620–626, 2017.

[5] Y. Zhang, Q. Z. Liu, S. P. Xing, and J. L. Zhang, "Inhibiting effect of Endostar combined with ginsenoside Rg3 on breast cancer tumor growth in tumor-bearing mice," *Asian Pacific Journal of Tropical Medicine*, vol. 9, no. 2, pp. 180–183, 2016.

[6] M. Mochizuki, Y. C. Yoo, K. Matsuzawa et al., "Inhibitory effect of tumor metastasis in mice by saponins, ginsenoside-Rb2, 20 (R)-and 20 (S)-ginsenoside-Rg3, of red ginseng," *Biological and Pharmaceutical Bulletin*, vol. 18, no. 9, pp. 1197–1202, 1995.

[7] I. H. Park, J. H. Sohn, S. B. Kim et al., "An open-label, randomized, parallel, phase III trial evaluating the efficacy and safety of polymeric micelle-formulated paclitaxel compared to conventional Cremophor EL-based paclitaxel for recurrent or metastatic HER2-negative breast cancer," *Cancer Research and Treatment*, vol. 49, no. 3, pp. 569–577, 2017.

[8] J. S. Suk, Q. Xu, N. Kim, J. Hanes, and L. M. Ensign, "PEGylation as a strategy for improving nanoparticle-based drug and gene delivery," *Advanced Drug Delivery Reviews*, vol. 99, Part A, pp. 28–51, 2016.

[9] I. A. Lázaro, S. Haddad, S. Sacca, C. Orellana-Tavra, D. Fairen-Jimenez, and R. S. Forgan, "Selective surface PEGylation of UiO-66 nanoparticles for enhanced stability, cell uptake, and pH-responsive drug delivery," *Chem*, vol. 2, no. 4, pp. 561–578, 2017.

[10] W. Li, P. Zhan, E. de Clercq, H. Lou, and X. Liu, "Current drug research on PEGylation with small molecular agents," *Progress in Polymer Science*, vol. 38, no. 3-4, pp. 421–444, 2013.

[11] H. Zhang, H. Hu, H. Zhang et al., "Effects of PEGylated paclitaxel nanocrystals on breast cancer and its lung metastasis," *Nanoscale*, vol. 7, no. 24, pp. 10790–10800, 2015.

[12] L. O. F. Monteiro, R. S. Fernandes, C. M. R. Oda et al., "Paclitaxel-loaded folate-coated long circulating and pH-sensitive liposomes as a potential drug delivery system: a biodistribution study," *Biomedicine & Pharmacotherapy*, vol. 97, pp. 489–495, 2018.

[13] C. Menzel, T. Holzeisen, F. Laffleur et al., "In vivo evaluation of an oral self-emulsifying drug delivery system (SEDDS) for exenatide," *Journal of Controlled Release*, vol. 277, pp. 165–172, 2018.

[14] A. A. Natfji, D. Ravishankar, H. M. I. Osborn, and F. Greco, "Parameters affecting the enhanced permeability and retention effect: the need for patient selection," *Journal of Pharmaceutical Sciences*, vol. 106, no. 11, pp. 3179–3187, 2017.

[15] J. Loureiro, S. Andrade, A. Duarte et al., "Resveratrol and grape extract-loaded solid lipid nanoparticles for the treatment of Alzheimer's disease," *Molecules*, vol. 22, no. 2, p. 277, 2017.

[16] H. Nosrati, M. Adibtabar, A. Sharafi, H. Danafar, and M. Hamidreza Kheiri, "PAMAM-modified citric acid-coated magnetic nanoparticles as pH sensitive biocompatible carrier against human breast cancer cells," *Drug Development and Industrial Pharmacy*, vol. 44, no. 8, pp. 1377–1384, 2018.

[17] H. Nosrati, E. Javani, M. Salehiabar, H. Kheiri Manjili, S. Davaran, and H. Danafar, "Biocompatibility and anticancer activity of L-phenyl alanine-coated iron oxide magnetic nanoparticles as potential chrysin delivery system," *Journal of Materials Research*, vol. 33, no. 11, pp. 1602–1611, 2018.

[18] M. Salehiabar, H. Nosrati, E. Javani et al., "Production of biological nanoparticles from bovine serum albumin as controlled release carrier for curcumin delivery," *International Journal of Biological Macromolecules*, vol. 115, pp. 83–89, 2018.

[19] H. Nosrati, R. Abbasi, J. Charmi et al., "Folic acid conjugated bovine serum albumin: an efficient smart and tumor targeted biomacromolecule for inhibition folate receptor positive cancer cells," *International Journal of Biological Macromolecules*, vol. 117, pp. 1125–1132, 2018.

[20] H. Nosrati, A. Rakhshbahar, M. Salehiabar et al., "Bovine serum albumin: an efficient biomacromolecule nanocarrier for improving the therapeutic efficacy of chrysin," *Journal of Molecular Liquids*, vol. 271, pp. 639–646, 2018.

[21] L. Roufegarinejad, A. Jahanban-Esfahlan, S. Sajed-Amin, V. Panahi-Azar, and M. Tabibiazar, "Molecular interactions of thymol with bovine serum albumin: spectroscopic and

molecular docking studies," *Journal of Molecular Recognition*, vol. 31, no. 7, article e2704, 2018.

[22] S. M. H. AL-Jawad, A. A. Taha, M. M. F. Al-Halbosiy, and L. F. A. AL-Barram, "Synthesis and characterization of small-sized gold nanoparticles coated by bovine serum albumin (BSA) for cancer photothermal therapy," *Photodiagnosis and Photodynamic Therapy*, vol. 21, pp. 201–210, 2018.

[23] B. White, A. Evison, E. Dombi, and H. E. Townley, "Improved delivery of the anticancer agent citral using BSA nanoparticles and polymeric wafers," *Nanotechnology, Science and Applications*, vol. 10, pp. 163–175, 2017.

[24] S. Thakur, N. Hashim, S. Neogi, and A. K. Ray, "Size-dependent adsorption and conformational changes induced in bovine serum albumin (BSA) on exposure to titanium dioxide (TiO_2) nanoparticles," *Journal of Separation Science*, vol. 52, no. 3, pp. 421–434, 2017.

[25] Y. Wen, H. Dong, Y. Li, A. Shen, and Y. Li, "Nano-assembly of bovine serum albumin driven by rare-earth-ion (Gd) biomineralization for highly efficient photodynamic therapy and tumor imaging," *Journal of Materials Chemistry B*, vol. 4, no. 4, pp. 743–751, 2016.

[26] P. Singh, Y. J. Kim, H. Singh, S. Ahn, V. Castro-Aceituno, and D. C. Yang, "In situ preparation of water-soluble ginsenoside Rh2-entrapped bovine serum albumin nanoparticles: in vitro cytocompatibility studies," *International Journal of Nanomedicine*, vol. 12, pp. 4073–4084, 2017.

[27] P. Singh, H. Singh, V. Castro-Aceituno, S. Ahn, Y. J. Kim, and D. C. Yang, "Bovine serum albumin as a nanocarrier for the efficient delivery of ginsenoside compound K: preparation, physicochemical characterizations and in vitro biological studies," *RSC Advances*, vol. 7, no. 25, pp. 15397–15407, 2017.

[28] H. Y. Cheung and Q. F. Zhang, "Enhanced analysis of triterpenes, flavonoids and phenolic compounds in *Prunella vulgaris* L. by capillary zone electrophoresis with the addition of running buffer modifiers," *Journal of Chromatography A*, vol. 1213, no. 2, pp. 231–238, 2008.

[29] J. Li and Y. Guo, "Basic evaluation of typical nanoporous silica nanoparticles in being drug carrier: structure, wettability and hemolysis," *Materials Science and Engineering: C*, vol. 73, pp. 670–673, 2017.

[30] L. Q. Thao, C. Lee, B. Kim et al., "Doxorubicin and paclitaxel co-bound lactosylated albumin nanoparticles having targetability to hepatocellular carcinoma," *Colloids and Surfaces B: Biointerfaces*, vol. 152, pp. 183–191, 2017.

[31] R. Yang, D. Chen, M. Li, F. Miao, P. Liu, and Q. Tang, "20(s)-ginsenoside Rg3-loaded magnetic human serum albumin nanospheres applied to HeLa cervical cancer cells in vitro," *Bio-Medical Materials and Engineering*, vol. 24, no. 6, pp. 1991–1998, 2014.

[32] X. Zheng, Z. Li, L. Chen, Z. Xie, and X. Jing, "Self-assembly of porphyrin–paclitaxel conjugates into nanomedicines: enhanced cytotoxicity due to endosomal escape," *Chemistry - An Asian Journal*, vol. 11, no. 12, pp. 1780–1784, 2016.

[33] I. S. Choi, C. M. Kim, and S. J. Jang, "Screening antibiotics using an Hoechst 33342 dye-accumulation assay to detect efflux activity in *Acinetobacter baumannii* clinical isolates," *Asian Biomedicine*, vol. 11, no. 4, pp. 371–378, 2018.

[34] Z. Yang, N. Sun, R. Cheng, C. Zhao, J. Liu, and Z. Tian, "Hybrid nanoparticles coated with hyaluronic acid lipoid for targeted co-delivery of paclitaxel and curcumin to synergistically eliminate breast cancer stem cells," *Journal of Materials Chemistry B*, vol. 5, no. 33, pp. 6762–6775, 2017.

[35] C. Tang, Y. Wang, Y. Long, X. An, J. Shen, and Y. Ni, "Anchoring 20(R)-ginsenoside Rg3 onto cellulose nanocrystals to increase the hydroxyl radical scavenging activity," *ACS Sustainable Chemistry & Engineering*, vol. 5, no. 9, pp. 7507–7513, 2017.

[36] R. Mathiyalagan, S. Subramaniyam, Y. J. Kim et al., "Synthesis and pharmacokinetic characterization of a pH-sensitive polyethylene glycol ginsenoside CK (PEG-CK) conjugate," *Bioscience Biotechnology and Biochemistry*, vol. 78, no. 3, pp. 466–468, 2014.

[37] A. Jahanban-Esfahlan, S. Dastmalchi, and S. Davaran, "A simple improved desolvation method for the rapid preparation of albumin nanoparticles," *International Journal of Biological Macromolecules*, vol. 91, pp. 703–709, 2016.

[38] H. Nosrati, M. Salehiabar, H. K. Manjili, H. Danafar, and S. Davaran, "Preparation of magnetic albumin nanoparticles via a simple and one-pot desolvation and co-precipitation method for medical and pharmaceutical applications," *International Journal of Biological Macromolecules*, vol. 108, pp. 909–915, 2018.

[39] S. Emami, H. Valizadeh, Z. Islambulchilar, and P. Zakeri-Milani, "Development and physicochemical characterization of sirolimus solid dispersions prepared by solvent evaporation method," *Advanced Pharmaceutical Bulletin*, vol. 4, no. 4, pp. 369–374, 2014.

[40] P. Singh, H. Singh, V. Castro-Aceituno et al., "Engineering of mesoporous silica nanoparticles for release of ginsenoside CK and Rh2 to enhance their anticancer and anti-inflammatory efficacy: in vitro studies," *Journal of Nanoparticle Research*, vol. 19, no. 7, p. 257, 2017.

[41] G. Kabay, C. Demirci, G. Kaleli Can, A. E. Meydan, B. G. Daşan, and M. Mutlu, "A comparative study of single-needle and coaxial electrospun amyloid-like protein nanofibers to investigate hydrophilic drug release behavior," *International Journal of Biological Macromolecules*, vol. 114, pp. 989–997, 2018.

[42] Y. Zu, L. Meng, X. Zhao et al., "Preparation of 10-hydroxycamptothecin-loaded glycyrrhizic acid-conjugated bovine serum albumin nanoparticles for hepatocellular carcinoma - targeted drug delivery," *International Journal of Nanomedicine*, vol. 8, pp. 1207–1222, 2013.

[43] N. B. N. N. Tran, F. Knorr, W. C. Mak et al., "Gradient-dependent release of the model drug TRITC-dextran from FITC-labeled BSA hydrogel nanocarriers in the hair follicles of porcine ear skin," *European Journal of Pharmaceutics and Biopharmaceutics*, vol. 116, pp. 12–16, 2017.